



Role of plastic anisotropy and its evolution on springback

Lumin Geng¹, R.H. Wagoner^{*}

*Department of Materials Science and Engineering, The Ohio State University, 177 Watts Hall,
2041 College Road, Columbus, OH 43210, USA*

Received 10 July 2000; received in revised form 24 July 2001

Abstract

Springback angles and anticlastic curvatures reported for a series of draw-bend tests have been analyzed in detail using a new anisotropic hardening model, four common sheet metal yield functions, and finite element procedures developed for this problem. A common lot of 6022-T4 aluminum alloy was used for all testing in order to reduce material variation. The new anisotropic hardening model extends existing mixed kinematic/isotropic and nonlinear kinematic formulations. It replicates three principal characteristics observed in uniaxial tension/compression test reversals: a transient region with low yield stress and high strain hardening, and a permanent offset of the flow stress at large subsequent strains. This hardening model was implemented in ABAQUS in conjunction with four yield functions: von Mises, Hill quadratic, Barlat three-parameter, and Barlat 1996. The simulated springback angle depended intimately on both hardening law after the strain reversal and on the plastic anisotropy. The springback angle at low back forces was controlled by the hardening law, while at higher back forces the anticlastic curvature, which depends principally on yield surface shape, controlled the springback angle. Simulations utilizing Barlat's 1996 yield function showed remarkable agreement with all measurements, in contrast to simulations with the other three yield functions. © 2002 Elsevier Science Ltd. All rights reserved.

Keywords: Springback; Sheet metal forming; Anticlastic curvature; 6022-T4 aluminum; HSLA steel; Draw-bend tests; Plastic anisotropy; Finite element modeling; Bauschinger effect; Anisotropic hardening; Nonlinear kinematic hardening; Isotropic hardening; Barlat yield function

1. Introduction

The use of aluminum alloys and high-strength steels to replace traditional steels increases the need for springback control because of their higher yield strength-to-elastic modulus ratios. In the current

^{*} Corresponding author. Tel.: +1-614-292-2079; fax: +1-614-292-6530.

E-mail address: wagoner.2@osu.edu (R.H. Wagoner).

¹ Current address: Project Engineer, VSAS Integration, GMNA, Pontiac Centerpoint Campus—Central, Mail code: 483-528-6B6, 2000 Centerpoint Parkway, Pontiac, MI 48341-3147, USA.

Nomenclature

c_p, γ	material parameters in the Armstrong–Frederick hardening rule
F_b	actual back force
\bar{F}_b	normalized back force
f	yield function
H^p	plastic modulus of the monotonic loading curve
H_c^p, H_r^p	the plastic moduli for continuous loading and reverse loading at the same equivalent plastic strain
m	mixed hardening factor
r	plastic anisotropy parameter
R	radius of sheet strip in the sidewall curl region
t	sheet thickness
α	center of the active yield surface
β	center of the bounding surface
σ_β	stress mapping point on the bounding surface
σ_0	size of the active yield surface
$\sigma_{\beta 0}$	size of the bounding surface
ρ	radius of sheet strip in contact with tooling before unloading
θ	overall springback angle of sheet strip
$\langle \sigma \rangle$	standard deviation
μ	friction coefficient

work, springback is considered in a draw-bend test that corresponds to the sidewall curl region of an industrial stamping, where the sheet undergoes bending and unbending with superimposed tension. After forming, the tools are removed and the part changes shape (elastically and perhaps plastically) to attain equilibrium with no imposed forces. Springback is thus an elastically-driven process that adjusts internal stresses to attain zero moment and force at each sheet location.

Accurate springback prediction requires sensitive and accurate numerical procedures and material modeling [1]. Numerical factors, such as integration scheme, element type and unloading scheme are more critical than for forming analysis [2–11]. Simple material parameters such as yield stress and work hardening rate have been evaluated [12–14], as has the use of superimposed tension, to control springback in practice [12,15]. The evolution of elastic modulus has been of concern [16–20]; in general springback is inversely proportional to the effective modulus.

The internal stress state at the end of forming depends on the plastic properties of the material and their evolution during forming. Cold-rolling induces preferred orientation of polycrystalline grains, and the texture-induced anisotropy can be assessed by measured plastic anisotropy parameters related to strains (r -values) or flow stresses, or can be predicted from texture measurements [21–23] using simple averaging rules [24,25].

Hill's quadratic yield function (Hill'48) [26,27] has been used widely in forming analysis although its application to metals with low r -values (such as aluminum alloys) has been criticized [28–30].

The quadratic version has been extended [31–33] by introducing high-order exponents and anisotropic material constants to provide more flexibility to obtain better agreement with tests.

A second line of yield functions was created [34,35] by fitting to polycrystalline calculations. Hosford's yield function [35] was derived in terms of principal stresses and normal anisotropy with exponents determined by the crystal structure [36–38]: typically 6 for BCC and 8 for FCC metals. Modifications include a plane-stress version [39] and one incorporating shear stresses [40]. Barlat extended the approach to include planar anisotropy [23,41], and later to a full three-dimensional orthotropy [30,42,43] based on a linear stress transformation [44] or two such transformations [45]. Recent modifications by Banabic et al. add parameters and flexibility [46–49] with enhanced ability to fit experimental measurements. In some studies [50], none of the yield functions have been found to be satisfactory, while in others [51], Barlat's 1996 yield function was found to be accurate for both r -values and yield stresses.

Sidewall springback is complicated by the stress reversal that occurs in the transition from bending to unbending as material flows over the die radius. Strain hardening, which mechanistically is related to the multiplication, annihilation, and multiplication of dislocations [52], may be considered to be equal in all directions, leading to the isotropic hardening assumption. Conversely, back stress fields that accumulate may have a directional effect on subsequent reverse deformation [53] leading to the observation of a Bauschinger effect [54–56]. Subsequent yield surfaces often show translation as well as distortion [57–68]. A wide variety of single crystal, polycrystalline, and multi-phase alloys exhibit Bauschinger effects [69–96].

In contrast to the extensive measurements of the Bauschinger effect in bulk materials, there is little data for in-plane deformation of sheet metals because of their propensity to buckle under uniaxial compression. Measurements have been conducted with simple shear tests [97,98], and in-plane reverse loading tests [99–101]. Balakrishnan [102] measured the uniaxial flow curves for three automotive body sheet alloys, including the subject of the current work, 6022-T4 aluminum. Transient hardening and permanent softening were observed for all three materials under uniaxial reverse loading. The magnitude of the stress offset and the transient strain range were found to vary with the prestrain.

The Bauschinger effect is not reproduced by standard isotropic hardening models. Anisotropic hardening models have been developed to reproduce characteristics of cyclic hardening behavior, including Mroz's multisurface theory [103,104], the two-surface models by Dafalias and Popov [105], and Krieg [106], and the Armstrong–Frederick type models [107,108]. The principal difference among these models is in the way of defining the generalized plastic modulus [109,110]. In two-surface or Mroz's multisurface model, the hardening modulus function and the translation direction are defined first, then the consistency condition is used to determine the magnitude of the yield surface translation. In the Armstrong–Frederick type model, the direction and magnitude of the yield surface translation are specified first, then the generalized plastic modulus is derived from the consistency condition. The major computational drawback of the two-surface model is the procedure for updating the distance between the stress loading point and the mapping point on the bounding surface. This updating procedure can lead to inconsistencies under complex loading conditions and multiaxial loads [109,111–114]. The multisurface model, with its piecewise linear response, however, cannot predict ratcheting or mean stress relaxation [109,114,115].

Various Armstrong–Frederick type hardening rules have been developed, many focusing on the decomposition of total back stresses and superimposition of several evolution rules [108,114,116–123]. Modification has also been made on the limiting surface of the Armstrong–Frederick type hardening

rule to allow a translating limiting surface [124–127]. Geng and Wagoner's two-surface plasticity model [127] reproduces the strain-hardening behavior from the in-plane compression–tension tests [102] of sheet metals. To model the permanent softening shown on reverse loading at larger prestrains, the bounding surface translates and expands concurrently according to a mixed hardening rule [128,129]. This model is similar to one introduced by Ohno et al. [124,125], except that the Ohno model involves sequential translation and expansion of the bounding surface following a path reversal. Application of the Geng–Wagoner hardening model to springback analysis improved [130–133] the prediction of draw-bend springback compared to isotropic hardening models.

In the current work, the Geng–Wagoner hardening law is implemented in conjunction with three anisotropic yield functions for 6022-T4 aluminum alloy. The resulting material models are used to simulate the draw-bend test and hence to assess the importance of anisotropy on springback and anticlastic curvature.

2. Material model

The Geng–Wagoner anisotropic hardening law was extended for use with three yield functional forms: Hill's [26,27] 1948 quadratic yield function, Barlat's [29] three-parameter yield function ("Barlat YLD89"), and Barlat's [30] seven-parameter yield function ("Barlat YLD96"). The needed hardening parameters were obtained by reanalysis of uniaxial tension–compression data presented elsewhere [102].

The yield surface anisotropy was fit to measured r -values obtained from tensile tests carried out at orientations of 0° , 45° , and 90° to the rolling direction. For Hill'48 and Barlat YLD89, r -values reported by Shen [134] were used as follows: $r_0 = 0.73$, $r_{45} = 0.44$, $r_{90} = 0.63$. For Barlat YLD96, a full set of constants have been presented [135] for the same lot of 6022-T4 aluminum alloy that was used for the tension–compression tests. Barlat YLD96 makes use of both r -values and yield stresses found from oriented tensile tests.

6022-T4 is a predominantly aluminum alloy with principal alloying elements Mg and Si, and small additions of Cu and other elements. It is intended for automotive body sheet applications. Processing includes a high-temperature solution heat treatment, a quench, and then natural aging. This is the condition in which the alloy was tested in the present work. (In commercial application, additional aging takes place in the paint-bake cycle of automobile manufacturing, after forming and joining operations are completed.) The grain size is $240 \mu\text{m}$ [102], the sheet thickness is 0.91 mm, and the yield stress is 172 MPa. Chemical composition, nominal mechanical properties, and uniaxial strain hardening equations have been presented in detail elsewhere [132,133].

3. Formulation of anisotropic hardening rule

Uniaxial tensile tests with strain reversals (i.e. tension–compression or compression–tension) typically show three principal features following the reversal. There is a transient region (over a limited strain range of the order of 0.01) consisting of a yield stress lower than the previous flow stress, followed by rapid strain hardening. In some cases, particularly after larger prestrains, there is also a long-term or "permanent" offset of the effective stress–strain curve from the monotonic one (the offset may be considered in terms of strain or stress) for large additional strains (of the order 0.10

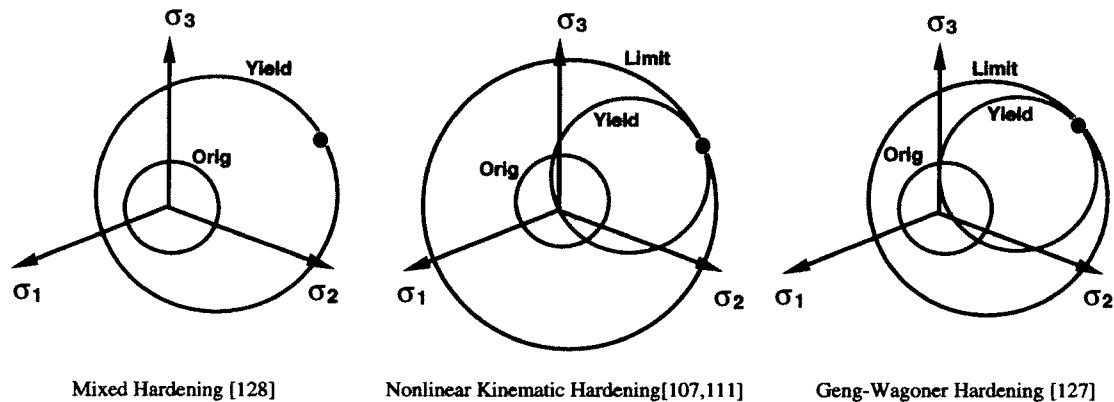


Fig. 1. Schematic comparison of anisotropic hardening models.

or greater). These characteristics are shown more explicitly in the next section for the 6022-T4 aluminum alloy.

Existing hardening laws are generally unable to reproduce this combination of features. Among the most common anisotropic hardening laws, the Hodge/Prager mixed hardening law [128,136] exhibits the long-term offset only while the Chaboche nonlinear kinematic hardening law [111] exhibits only the transient characteristics. The proposed anisotropic hardening law incorporates aspects of these models, and has similarities, as discussed later, to a model proposed by Ohno et al. [124,125]. A more complete derivation of the governing equations has been presented elsewhere [127].

The model is formulated starting from an assumed additive decomposition of the strain rate (or strain increment):

$$\dot{\boldsymbol{\epsilon}} = \dot{\boldsymbol{\epsilon}}^e + \dot{\boldsymbol{\epsilon}}^p. \quad (1)$$

The stress increment is related to the elastic strain rate as follows:

$$\dot{\boldsymbol{\sigma}} = \mathbf{C} \dot{\boldsymbol{\epsilon}}^e \quad (2)$$

and an associated flow rule is adopted:

$$\dot{\boldsymbol{\epsilon}}^p = \dot{\lambda} \frac{\partial f}{\partial \boldsymbol{\sigma}}, \quad (3)$$

where $\dot{\lambda}$ is an arbitrary scalar constant determined by consistency of the flow rule, and f is the yield function.

Fig. 1 illustrates the principles of the new hardening model as compared to existing ones. The new hardening model is a modification of one proposed by Armstrong and Frederick [107] and developed by Chaboche [111]. These “nonlinear kinematic hardening” models can be considered two-surface formulations [111] starting from classic kinematic hardening ideas of Prager and Ziegler. The new modification uses the similar rules for the active yield surface, but allows the bounding surface to develop according to a mixed hardening law [128,129], rather than by an isotropic expansion in Chaboche’s implementation. This modification allows replication of both the transient response following a path change via the motion of the active yield surface and a permanent offset via the bounding surface development.

The new hardening rule may be expressed as in the Armstrong–Frederick formulation with an additional term to allow for translations and expansion of the limiting or bounding surface:

$$d\boldsymbol{\alpha} = \frac{c_p}{\sigma_0}(\boldsymbol{\sigma} - \boldsymbol{\alpha}) d\varepsilon^p - \gamma(\boldsymbol{\alpha} - \boldsymbol{\beta}) d\varepsilon^p, \quad (4)$$

where $d\varepsilon^p$ is the equivalent plastic strain rate; and σ_0 , c_p and γ are material parameters, with σ_0 representing the yield surface size. $\boldsymbol{\beta}$ is the center of the bounding surface. Following the assumptions in Dafalias and Popov's two-surface model [105] and Mroz's model [103,104], the stress mapping point $\boldsymbol{\sigma}_\beta$ on the bounding surface is determined as follows:

$$\boldsymbol{\sigma}_\beta - \boldsymbol{\beta} = \frac{\sigma_{\beta 0}}{\sigma_0}(\boldsymbol{\sigma} - \boldsymbol{\alpha}), \quad (5)$$

where $\sigma_{\beta 0}$ represents the size of the bounding surface. The translation and expansion of the bounding surface is specified with a mixed hardening rule [128,129]:

$$d\boldsymbol{\beta} = \frac{mH^p}{\sigma_{\beta 0}}(\boldsymbol{\sigma}_\beta - \boldsymbol{\beta}) d\varepsilon^p \quad (6)$$

and

$$d\sigma_{\beta 0} = (1 - m)H^p d\varepsilon^p, \quad (7)$$

where H^p is the plastic modulus of the monotonic loading curve, and m is the ratio of the kinematic response (translation) to the isotropic response (expansion) of the bounding surface. If $\boldsymbol{\beta} = \mathbf{0}$, the nonlinear kinematic hardening law of Chaboche [111] is recovered; whereas if $\boldsymbol{\beta} = \boldsymbol{\alpha}$, the mixed hardening law of Hodge [128,129] is obtained. The material parameters can be calibrated from the experimental uniaxial tension/compression measurements.

The active yield function is expressed as follows:

$$f(\boldsymbol{\sigma} - \boldsymbol{\alpha}) - \sigma_0 = 0. \quad (8)$$

For uniaxial loading, using a consistency condition, the plastic modulus can be expressed as follows:

$$H^p = \frac{d\sigma}{d\varepsilon^p} = c_p - \gamma(\alpha - \beta)\text{Sgn}(\sigma - \alpha) + \frac{d\sigma_0}{d\varepsilon^p}, \quad (9)$$

where $\text{Sgn}(x) = 1$ if $x > 0$, or $\text{Sgn}(x) = -1$ if $x < 0$.

For a uniaxial tensile loading followed by uniaxial compressive reversal, the plastic modulus can become much higher at the onset of the stress reversal because of the sign change of the second term in Eq. (9). The material parameters c_p and γ can be determined by the initial reverse flow modulus:

$$c_p = \frac{H_c^p(\varepsilon^p) + H_r^p(\varepsilon^p)}{2} - \frac{d\sigma_0}{d\varepsilon^p} \quad (10)$$

and

$$\gamma = \frac{H_r^P(\varepsilon^P) - H_c^P(\varepsilon^P)}{2(\alpha - \beta)}, \quad (11)$$

where H_c^P and H_r^P are the plastic moduli for continuous loading and reverse loading at the same equivalent plastic strain. It can be seen from Eqs. (10) and (11) that both parameters are functions of the deformation history (characterized by effective plastic strain ε^P).

It should be noted that Eqs. (4)–(7) are similar to ones presented by Ohno [124,125]. Both Geng–Wagoner and Ohno models are based on two-surface formulations introduced previously in various forms [103–106]. Both models consider isotropic and kinematic hardening of the bounding surface to represent the long-range plastic deformation after a path reversal. The transient hardening immediately following the reversal is represented by the yield surface evolution within the bounding surface.

There are several differences, however. The most important involves the evolution of the bounding surface. Ohno's model invokes a sequence of first combined hardening and then purely kinematic hardening of the bounding surface following a strain reversal. Multiple loading cycles can then be fit by allowing the transition strain to vary with the number of cycles. Geng and Wagoner's model invokes concurrent kinematic and isotropic evolution of the bounding surface, with no provision in the current version for multiple loading cycles. Ohno's model, for simplicity, assumes a yield surface of a constant size and treats other material parameters, except for the transition strain, as constants. Geng and Wagoner's model allows material parameters to evolve as simple, piecewise linear functions of effective strain (related to the current flow stress for uniaxial loading). Thus, Ohno's model offers a method for handling multiple cycles, with penalties for (a) additional parameters needed to be fit by experiment, and (b) ignoring evolution of the transient response following various proportional path lengths (prestrains). Geng and Wagoner's model has fewer parameters and thus may be fit with one or more single loading cycles. However, it has no current provision to capture the saturation of transient response seen after numerous loading cycles.

4. Fit of hardening law to experimental data

In-plane tension compression tests were developed and carried out for 6022-T4 aluminum alloy [102] to reveal the characteristics of the Bauschinger effect. The material parameters of the proposed hardening model were obtained by fitting these uniaxial reverse loading curves. In Eqs. (10) and (11), the parameter H_c^P is determined from the monotonic loading curve, while H_r^P can be obtained by fitting to the initial hardening slope at the onset of the reverse plastic flow. The term $\alpha - \beta$ in Eq. (11) can be defined by knowing the size of the bounding surface and the active yield surface. The bounding surface size is determined by the mixed hardening factor (m -value) and its evolution with prestrain, while the m -value can be characterized by the amount of permanent softening on the reverse flow curve. The reverse flow curve is thus determined by the parameters m , c_p and γ , together with evolution functions of these three parameters with prestrain. A trial-and-error procedure was used to find the best-fit material parameters.

A stress–strain curve for a typical uniaxial tension–compression experiment [102] for 6022-T4 aluminum alloy is presented in Fig. 2, with a monotonic uniaxial tension curve for comparison. The

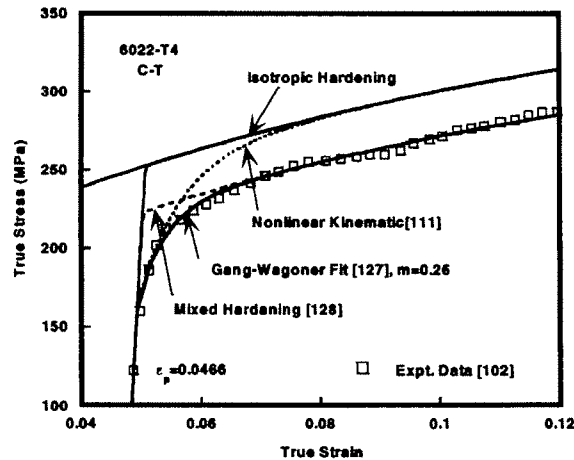


Fig. 2. Fit of anisotropic hardening laws to uniaxial tension–compression data [102] for 6022-T4 aluminum alloy: isotropic hardening, mixed hardening [128], nonlinear kinematic hardening [111], and Geng–Wagoner hardening [127].

curve following the reversal shows the three characteristics described earlier: a transient region with low yield stress and rapid work hardening, and a persistent offset of the flow stress (or, equivalently, a strain offset) from the isotropic hardening curve. Fig. 2 illustrates the fit of standard hardening models to these data compared with a Geng–Wagoner model. Isotropic hardening reproduces none of the Bauschinger effect, mixed hardening reproduces the stress offset but not the transient characteristics, and the Chaboche model reproduces the transient region but not the persistent offset. Both the transient and large-strain characteristics following the stress reversal are reproduced adequately by the Geng–Wagoner model.

It should be noted that a better fit can be obtained using the Chaboche model by dividing the back stress into multiple values and allowing each component to evolve at a different rate (as proposed by Chaboche [111]). This approach can produce a transient shape better matching the experimental results (at the expense of additional fitting). However, at large strains following the reversal the flow stress must still approach the monotonic curve. That is, the entire subsequent hardening is treated as a transient response that gradually disappears, leaving the monotonic response. The apparently permanent recovery shown by the experimental data in Fig. 2 cannot thus be reproduced by even multiple transients of this kind. Ohno's model was not compared because fitting it requires multiple-cycle testing that was not available.

Uniaxial tension/compression test data are available from tension–compression or compression–tension tests at three or four prestrain values, ranging from 1% to 8%. Trial functions of variations of these material parameters with prestrain were first created from the measurements of the reverse flow curve; then a theoretical reverse flow curve was calculated. Depending on the fitting results, the parameters were adjusted accordingly. Curve fitting was performed one-by-one on the test data at different prestrains, with each parameter calibrated at three or four prestrains. Two sets of material parameters, labeled the C–T (for compression–tension) model and T–C (for tension–compression) model, were obtained for each material based on the uniaxial compression/tension test data, Fig. 3.

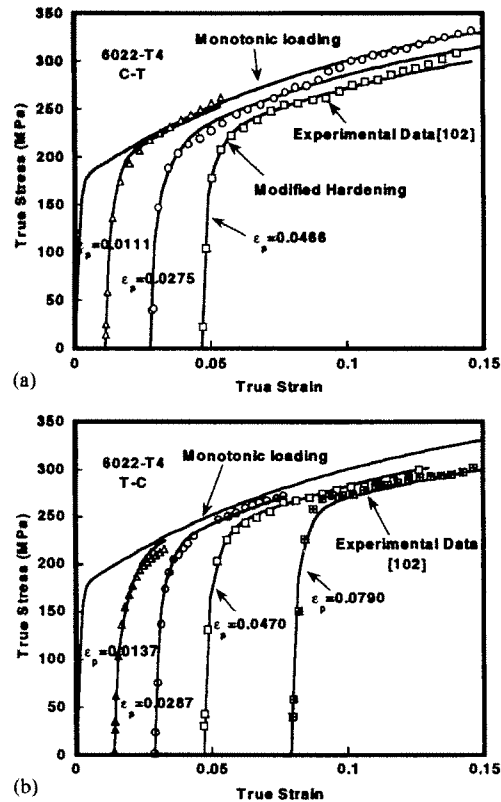


Fig. 3. Geng–Wagoner hardening law compared with measurements for 6022-T4 aluminum alloy for several prestrains: (a) uniaxial compression–tension; and (b) uniaxial tension–compression.

Fig. 4 shows the calibrated functions of material parameters with respect to prestrain. In the figure, calibrated values of reverse yield stress, bounding surface size and H_r^p at various prestrains are plotted. Each data point comes from fitting to each reverse flow curve. Piecewise linear interpolation was used between the determined material parameter points. For the material parameters at strains higher than the measured strain range, the value of m and H_r^p are taken to be the same as those measured at the highest prestrain available; and the rate of active yield surface expansion is assumed to be the same as that of the bounding surface.

5. Yield functions

To take into account the planar anisotropy of rolled metal sheets, the hardening model was extended to include three anisotropic yield criteria: Hill'48 [26,27], Barlat's three-parameter yield function (Barlat YLD89) [29] and Barlat's YLD96 [30]. Only the plane stress condition, appropriate for thin shell elements, was modeled.

Hill's quadratic yield function [26,27] was developed to account for the orthotropic symmetry of rolled metal sheets. Although its use is controversial for materials with low r -value [13,17], it

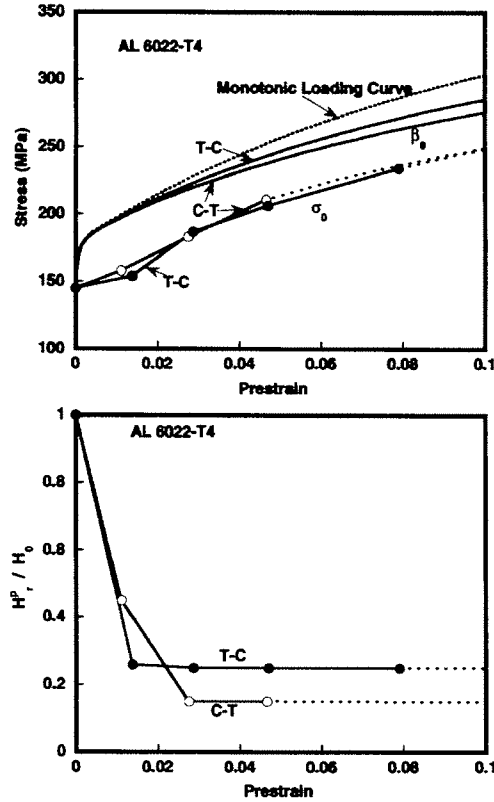


Fig. 4. Anisotropic hardening parameters obtained by fitting to experimental uniaxial tension/compression data [102]. The value of H_0 is 114 GPa.

has been widely used with finite element modeling because of the relative ease of formulation. Considering back stress terms, the yield function can be expressed as follows:

$$f(\boldsymbol{\sigma} - \boldsymbol{\alpha}) - \sigma_0 = (F\mathbf{s}_y^2 + G\mathbf{s}_x^2 + H(\mathbf{s}_x - \mathbf{s}_y)^2 + 2N\mathbf{s}_{xy}^2)^{1/2} - \sigma_0 = 0, \quad (12)$$

where, $\mathbf{s} = \boldsymbol{\sigma} - \boldsymbol{\alpha}$. F , G , H and N are material constants, which are typically determined from r -values measured at 0° , 45° and 90° from the rolling direction: $r_0 = 0.73$, $r_{45} = 0.44$, $r_{90} = 0.63$ [134]. The r -values at angle θ from the rolling direction can be expressed as follows:

$$r_x = \frac{H + (2N - F - G - 4H) \sin^2 \theta \cos^2 \theta}{F \sin^2 \theta + G \cos^2 \theta}, \quad (13)$$

from which the parameters in Hill's yield function can be determined as follows:

$$F = \frac{r_0}{r_{90}(1 + r_0)} = 0.67, \quad G = \frac{1}{1 + r_0} = 0.58, \quad H = \frac{r_0}{1 + r_0} = 0.42$$

and

$$N = \frac{(r_0 + r_{90})(1 + 2r_{45})}{2r_{90}(1 + r_0)} = 1.17. \quad (14)$$

Barlat et al. [29] proposed a modification of Hosford's isotropic yield function [35,36]. Anisotropic material parameters were introduced and a shear stress term included. This surface can be extended to include the back stress term:

$$f(\boldsymbol{\sigma} - \boldsymbol{\alpha}) - \sigma_0 = \left\{ \frac{1}{2}(a|K_1 + K_2|^n + a|K_1 - K_2|^n + c|2K_2|^n) \right\}^{1/n} - \sigma_0 = 0, \quad (15)$$

where

$$K_1 = \frac{s_x + hs_y}{2} \quad (16)$$

and

$$K_2 = \sqrt{\left(\frac{s_x - hs_y}{2} \right)^2 + p^2 s_{xy}^2}, \quad (17)$$

in which a , c , h , and p are material constants introduced into formulation to account for planar anisotropy. These parameters can be calculated either by flow stress (uniaxial flow stress, shear flow stress or biaxial flow stress) at different orientations, or by r -values at 0° , 45° and 90° from the rolling direction. In this study, the second approach [29] was used:

$$a = 2 - c = 2 - 2\sqrt{\frac{r_0}{1+r_0} \frac{r_{90}}{1+r_{90}}} = 1.19, \quad (18)$$

$$h = \sqrt{\frac{r_0}{1+r_0} \frac{1+r_{90}}{r_{90}}} = 1.04. \quad (19)$$

The value of p cannot be calculated explicitly. However, the r -values at an angle of θ to the rolling direction can be expressed as follows:

$$r_\theta = \frac{2m\sigma_0^n}{(\partial f / \partial \sigma_x + \partial f / \partial \sigma_y)\sigma_\theta} - 1, \quad (20)$$

where σ_θ is the uniaxial flow stress in the angle of θ from the rolling direction. Typically r_{45} is used with this equation to iteratively determine the value of p , which is 0.947 in this case.

Barlat et al. [30] developed a more general yield function to describe the planar anisotropy of aluminum alloy sheets. For plane stress conditions, this function can be expressed as follows:

$$f(\boldsymbol{\sigma} - \boldsymbol{\alpha}) - \sigma_0 = \left\{ \frac{1}{2}(\alpha_3|S_1 - S_2|^n + \alpha_1|S_2 - S_3|^n + \alpha_2|S_3 - S_1|^n) \right\}^{1/n} - \sigma_0 = 0. \quad (21)$$

where S_i are the principal values of the symmetric matrix \mathbf{S}_{ij} :

$$\mathbf{S}_{ij} = \begin{bmatrix} S_{xx} & S_{xy} & 0 \\ S_{xy} & S_{yy} & 0 \\ 0 & 0 & S_{zz} \end{bmatrix} \quad (22)$$

and where

$$S_{xx} = \frac{C_3(s_x - s_y) + C_2s_x}{3}, \quad (23)$$

$$S_{yy} = \frac{C_1s_y - C_3(s_x - s_y)}{3}, \quad (24)$$

$$S_{xy} = C_6s_{xy}. \quad (25)$$

C_1 , C_2 , C_3 and C_6 are material constants, and α_1 , α_2 and α_3 can be expressed as

$$\alpha_1 = \alpha_x \cos^2 2\theta + \alpha_y \sin^2 2\theta, \quad (26)$$

$$\alpha_2 = \alpha_x \sin^2 2\theta + \alpha_y \cos^2 2\theta, \quad (27)$$

$$\alpha_3 = \alpha_{z0} \cos^2 2\theta + \alpha_{z1} \sin^2 2\theta. \quad (28)$$

Typically $\alpha_{z0} = 1$, and θ is the angle between S_1 and the rolling direction.

The material constants C_1 , C_2 , C_3 , C_6 and α_x , α_y , α_{z1} can be determined by tensile yield stress and r -values measured at 0° , 45° and 90° from the rolling direction, along with the balanced biaxial flow stress measured by the bulge test [30,135]. The recommended n -value is 8 for FCC materials and 6 for BCC materials. For the 6022-T4 aluminum alloy used in this study, the appropriate coefficients have been determined elsewhere [135] as follows: $C_1=0.9243$, $C_2=0.7967$, $C_3=1.0458$, $C_6=1.0590$ and $\alpha_x = 3.25$, $\alpha_y = 3.30$, $\alpha_{z1} = 0.45$.

6. Simulation of the draw-bend test

In order to test the accuracy of the derived constitutive models, simulations of the draw-bend test were carried out using ABAQUS [137] and compared with existing experimental results [132,133]. The material models were implemented via the UMAT interface of ABAQUS utilizing a backward Euler algorithm [129] for integration of the incremental plasticity equations and a consistent tangent matrix derived from this algorithm for Newton–Raphson iteration.

The draw-bend test, shown schematically in Fig. 5, was designed for the measurement of friction [130]. A constant resisting force (expressed as a fraction of the force to yield the sheet in tension) is applied to the upper leg and the lower leg is drawn at a speed of 40 mm/s for a distance of 127 mm. The specimens are oriented along the sheet rolling direction, and are 50.8 mm wide. When the specimen is under load in the grips at the end of the draw, the angle between the legs is 90° , the radius of curvature in contact with the rod is nominally the rod radius (ρ), and the radius of the drawn length of the specimen (R) is infinite, i.e. it is straight. Upon removal of the specimen from the grips, the included leg angle changes by $\Delta\theta$, the contact radius of the sheet becomes ρ' , and the radius of the drawn length (i.e. the “sidewall curl region” in industrial parlance) becomes R' .

Experimental results [132,133] for three sheet alloys, including 6022-T4 aluminum, show that the magnitude of $\Delta\theta$ is dominated by the response of the sidewall curl region (i.e. R'), and that this

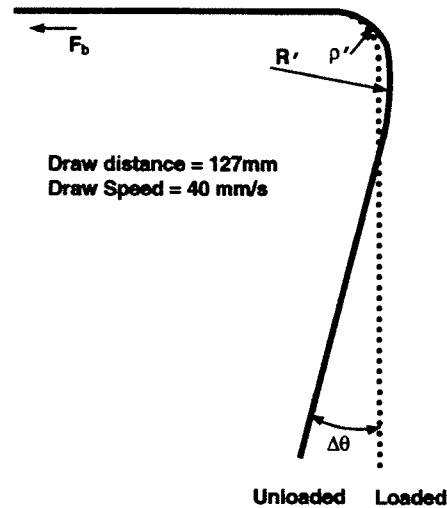


Fig. 5. Schematic of draw-bend test as implemented for springback measurement.

quantity can be measured more accurately than the radii of curvature. (The measurement reproducibility of 0.2° corresponds to a strain difference of 0.001% at the outer fiber of the sidewall curl region [133].) The results also show that significant anticlastic curvature² occurs with the 6022-T4 alloy (50.8 mm width specimens were used throughout) for back forces in the range of 0.8–1.2 times the yield force. Therefore, three-dimensional modeling is required in spite of the nominally two-dimensional nature of the problem.

Simulation of the draw-bend test using isotropic hardening and, an isotropic yield function has been carried out and reported elsewhere [140]. Sensitivity studies [11,140,141] showed that special care of numerical tolerances and mesh configurations must be taken to obtain accurate solutions after springback. These results were used to configure the simulations reported here. The mesh consists of fine elements where contact is made with the tooling (226 elements \times 0.62 mm original length, the turning angle for each element in contact with the tools in this mesh is 3.8°) and coarse elements in the straight legs away from contact (39 elements \times 5.2 mm original length). Along the width direction, 8 equal-sized elements are used in the half-width of the specimen. The springback step is elastic–plastic, as plastic deformation can occur during this elastically-driven process [140]. A friction coefficient of 0.15 was adopted throughout, consistent with experiments that showed a range of results from 0.12 [133] to 0.15 [132].

² Anticlastic curvature [138,139] is the secondary curvature orthogonal to the principal curvature. It occurs because of differential lateral contraction from the top of the sheet to the bottom under the principal bending action. However, in the draw-bend test, the principal and secondary curvatures are typically concave toward the tool contact side of the strip, which violates the formal definition of “anticlastic”, although this term has acquired the meaning of a secondary, orthogonal curvature resulting from a primary bending. The proper term would be “synclastic” because the concavity of the two curvatures is on the same side of the sheet.

7. Results and discussion

Fig. 6 shows the simulated springback angles ($\Delta\theta$) for a range of back forces and for four yield functions. In each case, the Geng–Wagoner anisotropic hardening models derived from tension–compression (T–C) and compression–tension tests (C–T) are compared with isotropic hardening.

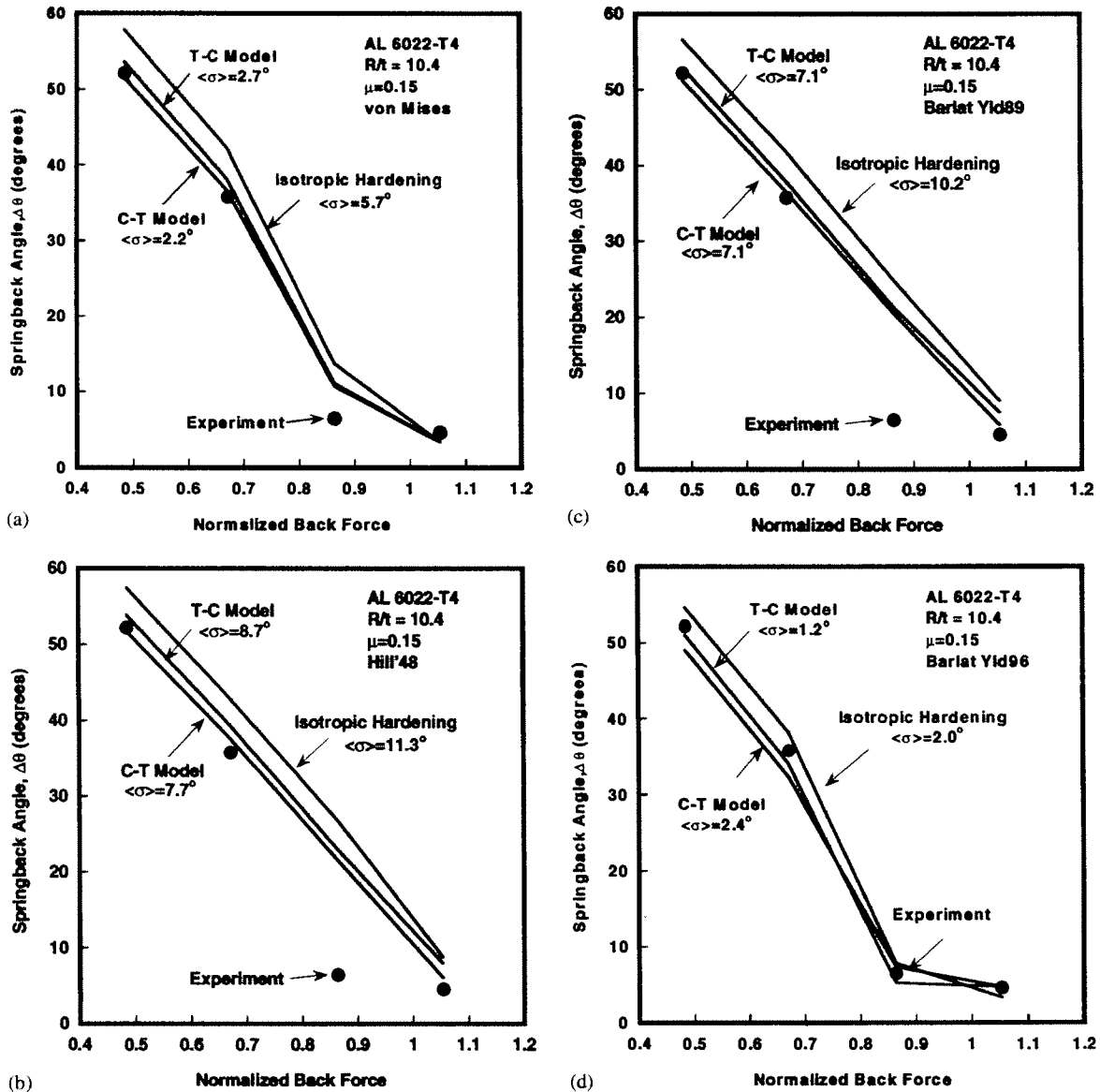


Fig. 6. Comparison of measured springback angles with simulations using isotropic or anisotropic hardening and four yield functions: (a) von Mises; (b) Hill'48; (c) Barlat YLD89; and (d) Barlat YLD96. $\langle\sigma\rangle$ represents the standard deviation of simulated and measured angles.

For all four yield functions, springback predictions are in better agreement with experimental measurements for the Geng–Wagoner hardening model. At lower back forces, the springback angle is more sensitive to the hardening model: a 5–9° reduction of $\Delta\theta$ is predicted for the modified hardening model. At high back forces, the springback angle is more sensitive to the yield surface type, especially for the back forces close to yield.

For the models with the Hill'48 yield surface (Fig. 6b) or Barlat YLD89 yield surface (Fig. 6c), the simulated springback angle tends to linearly decrease relative to the increasing back force, with consequent large errors at intermediate back forces (near yield). However, the springback angles predicted by the material models with von Mises (Fig. 6a) and Barlat YLD96 (Fig. 6d) show a trend similar to the experimental measures: a rapid decrease in springback for normalized back forces near 0.9, with a plateau thereafter. In particular, the model with the Barlat YLD96 yield surface and modified hardening predicts a springback angle at back force of 0.9 very close to the experimental value.

The measured rapid drop [131–133] of the springback angle at back forces near yield is associated with the appearance of significant secondary curvature (anticlastic curvature) [133], Fig. 7. Anticlastic curvature increases the moment of inertia of the sheet cross section, which reduces the bending of the sheet strip during springback, thus causing the precipitous drop of springback. In Fig. 7, the data for six repeated experiments carried out at $F_b = 0.9$ are shown to illustrate the scatter. (In Fig. 6 and in subsequent figures, the multiple experimental results for $F_b = 0.9$ are lumped into a single point and the experimental result for $F_b = 1.3$ is not shown because it was not possible to obtain converged FEA solutions for this case for comparison.) The difference in anticlastic curvature between C–T and T–C derived hardening models is insignificant. In plots comparing anticlastic curvatures, only the C–T results are shown.

The simulated anticlastic curvature, both in the loaded and unloaded states, depends little on the details of the hardening model (i.e. the presence of a Bauschinger effect versus isotropic hardening); instead it is closely related to the magnitude of the back force and the form of the yield function. In contrast, the simulated springback angle is influenced significantly by both aspects of the constitutive equation. This distinction provides an intriguing capability to discriminate both yield surface anisotropy and strain ratio anisotropy using a single experiment.

The simulated anticlastic curvature under load (i.e. before springback) decreases slowly with increasing back force for all yield functions and hardening laws, Fig. 8a–d. However, there are marked differences in the behavior of the anticlastic curvature after springback. (The anticlastic curvature in the unloaded state following forming is referred to here as “persistent anticlastic curvature”.) For von Mises and Barlat YLD96 yield functions, Fig. 8a and d, the persistent anticlastic curvature shows a sudden, large increase as the back force approaches the yield force, in agreement with measurements. It appears that once this transition is made, the anticlastic curvature remains approximately constant for higher back forces. The jump of persistent anticlastic curvature obtained with these two yield functions corresponds to the simulated and measured rapid decreases of springback angle.

For Hill'48 and Barlat YLD89, the persistent anticlastic curvature increases more gradually and the transition to persistence occurs at higher back forces, in contrast to the measured behavior. The corresponding springback angle variation with back force for these yield surfaces (Fig. 6b and c) are continuous and approximately linear instead of showing a sudden decrease near the yield force.

The Barlat YLD96 yield function reproduces both springback angles and anticlastic curvatures in remarkable agreement with measured values and variations. The von Mises isotropic yield function

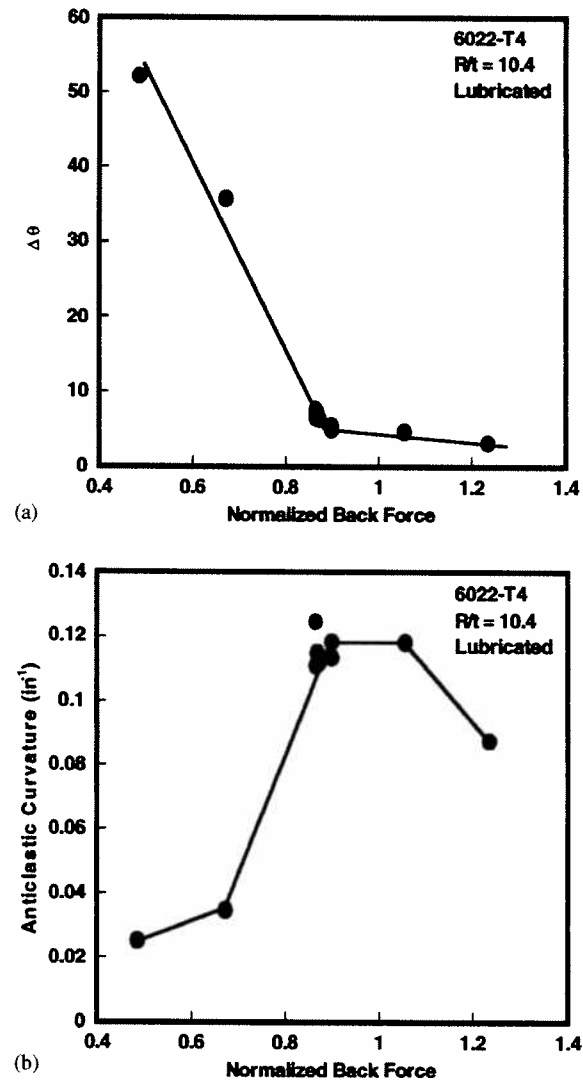


Fig. 7. Variation of measured draw-bend test quantities with the back force: (a) springback angle; and (b) anticlastic curvature.

is better than the remaining anisotropic yield functions, in spite of having no adjustable parameters corresponding to anisotropy.

Fig. 9a shows the variation of plastic anisotropy parameter with orientation for the four yield functions as compared with measured values from tensile tests. Barlat YLD96 and Hill'48 are nearly identical throughout the range whereas Barlat YLD89 differs near the transverse direction. As shown, multiple measurements of r -value (r = plastic anisotropy parameter) were reported, with the values of Shen [134] used to fit Barlat YLD89 and Hill'48, and the values of Barlat [135] used to fit Barlat YLD96, hence the slightly different results.

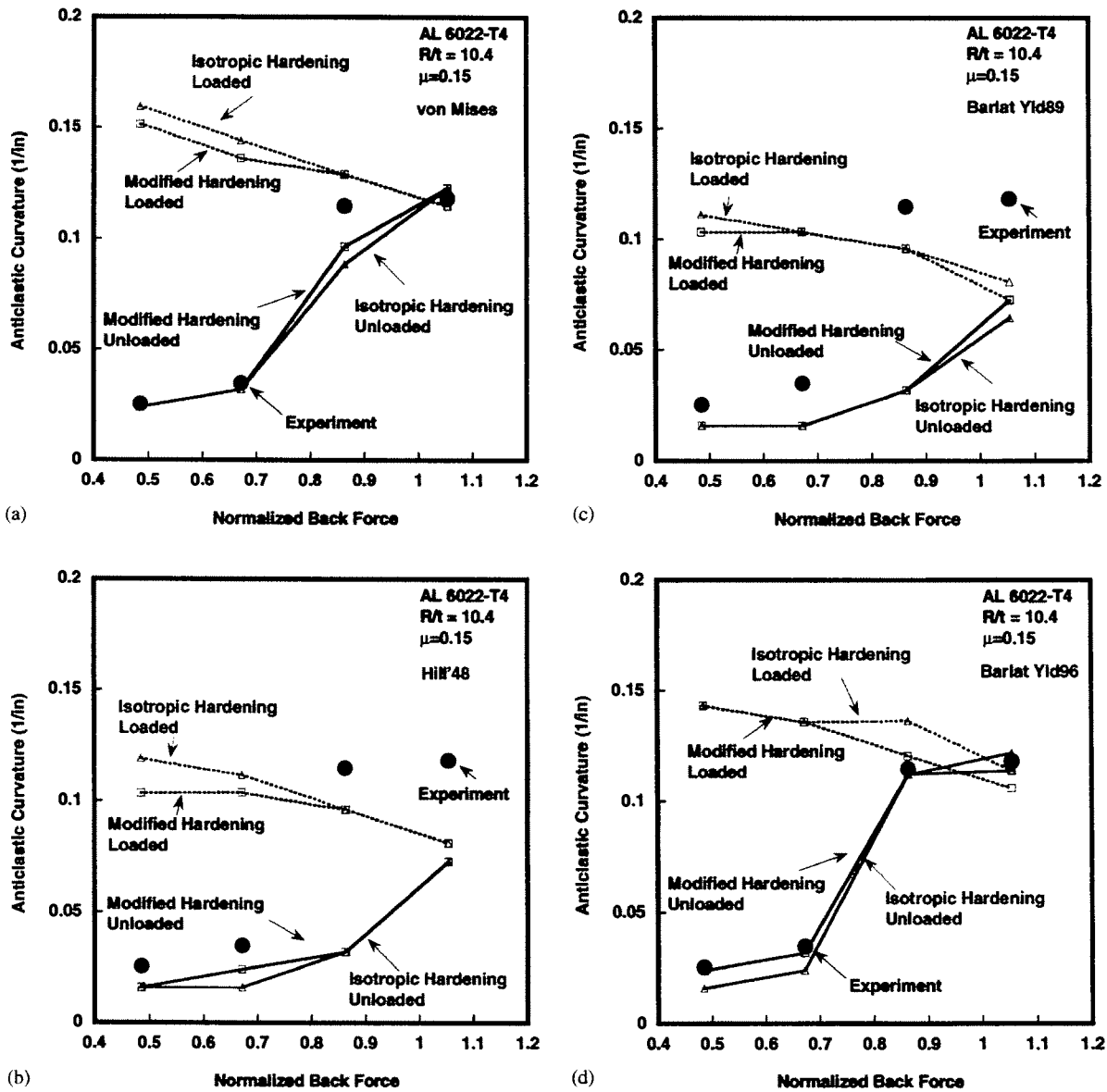


Fig. 8. Comparison of measured anticlastic curvatures with simulations using isotropic or anisotropic hardening and four yield functions: (a) von Mises; (b) Hill '48; (c) Barlat YLD89; and (d) Barlat YLD96.

Fig. 9b shows the variation of tensile yield stress with orientation for the four yield functions. Hill'48 and Barlat YLD89 are similar, with Barlat YLD96 quite different, having nearly the opposite variation near 45° . Of course, there is no variation for the isotropic von Mises law. Comparison with experiment reveals that only Barlat YLD96 captures the variation adequately in comparison to oriented tensile tests.

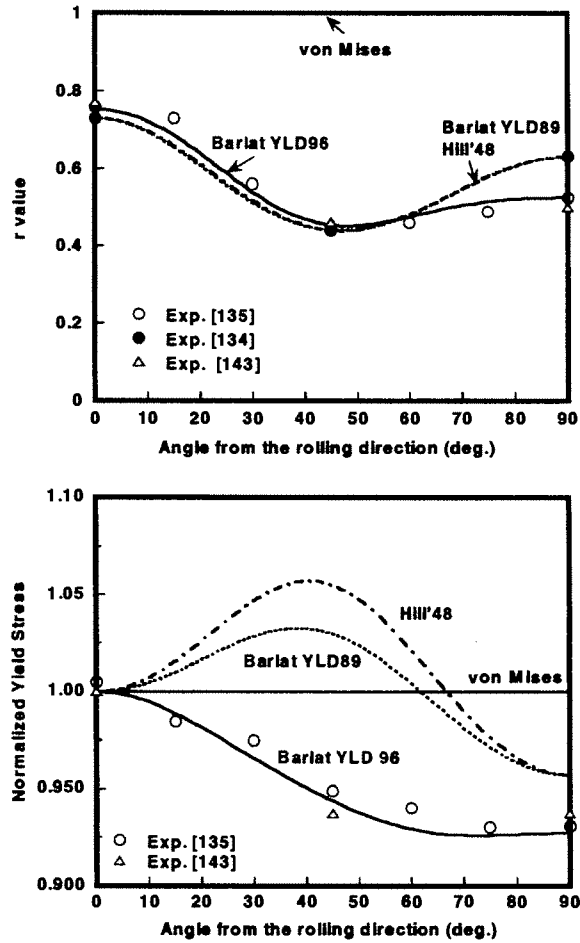


Fig. 9. Comparison of measured and fit *r*-values and yield stresses for four yield functions.

The two parts of Fig. 9 provide insight into the performance of the four yield functions in simulating draw-bend springback and anticlastic curvature. Because the long axis of the draw-bend specimen is oriented parallel to the rolling direction of the sheet, the stresses producing the internal bending moment are parallel to the rolling direction. As shown in Fig. 9b, these stresses will be identical for the various models under the same kinematic constraints. However, the lateral contraction of the sheet is related to *r*-value in the rolling direction (r_0) as follows: (width strain/principal bending strain) = $-r_0/(1+r_0)$, assuming plane stress conditions. While the three anisotropic yield functions have virtually identical r_0 values of 0.73, the von Mises value of 1 is considerably higher, hence the lateral contraction and anticlastic curvature would be expected to be considerably larger.

In addition to strain ratios, the lateral yield stress (i.e. the yield stress at 90° to the sheet rolling direction, i.e. in the sheet transverse direction) affects anticlastic curvature in two ways. A higher lateral yield stress and correspondingly higher lateral yield strain (the value of which may be obtained

via the elastic constants) resists the development of anticlastic curvature during forming because for a given lateral strain (with an assumed plastic component), the resisting stress is larger. For a given loaded anticlastic curvature, a higher lateral yield stress reduces the persistent anticlastic curvature by increasing the magnitude of the elastic unloading strains. Since Hill'48 and Barlat YLD89 are nearly identical in both r -value distribution and transverse yield stress, the simulated anticlastic curvature and springback angles with these yield functions would be expected to be very similar, as confirmed by Fig. 6b and c, and Fig. 8b and c.

For Barlat YLD96, the r_0 value is the same as for the other anisotropic yield functions, but the yield stress in the transverse direction is considerably lower (Fig. 9b). Therefore, one would expect higher anticlastic curvature in both the loaded and unloaded states, with concurrent reductions in springback angle. These expectations are confirmed by comparing Fig. 6d with Fig. 6b and c, and Fig. 8d with Fig. 8b and c.

For the von Mises yield function, there is an off-setting of tendencies. The considerably higher r_0 value tends to increase anticlastic curvature, but the transverse yield stress is much higher, thus tending to reduce the anticlastic curvature. These two effects nearly balance such that the springback angles are reasonably well predicted (Figs. 6a and 8a) by this less accurate yield function (as shown in Fig. 9a and b). At a back force of 0.9, the larger recovery of anticlastic curvature can be seen for the von Mises yield function as compared with Barlat YLD96, Fig. 8a and d. This is presumably a result of the much higher transverse yield stress exhibited by the von Mises yield function, such that there is little persistent anticlastic curvature until higher back forces are reached.

It is clear that the planar anisotropy of sheet metal is an important factor influencing springback which involves anticlastic curvature. The draw-bend test has interesting features to recommend it for investigation of both springback and elastic–plastic constitutive equations. Very fine strain resolution is possible, to approximately 0.001%, and the test is easy and fast to carry out. The springback angle and anticlastic curvature depend intimately on both yield surface shape and Bauschinger effect/anisotropic hardening. When combined with a series of oriented tensile tests, it is possible to obtain a clear picture of the accuracy of common yield functions.

8. Conclusions

Reported springback angles and anticlastic curvatures measured using draw-bend tests [132,133] have been reanalyzed using finite element modeling techniques developed for this test [11,140–142] in conjunction with highly developed constitutive equations for 6022-T4 aluminum alloy. The constitutive equations incorporate (a) a new anisotropic hardening rule [127] fit to tension–compression data appearing in the literature [102] for this particular lot of alloy, and (b) four yield functions (von Mises, Hill'48 [26,27], Barlat's three-parameter yield function (Barlat YLD89) [29] and Barlat's YLD96 [30]) fit to oriented tensile data for this lot of alloy.

The following conclusions were reached:

1. The draw-bend test is particularly well-suited to the investigation of springback and constitutive behavior because springback angle and anticlastic curvature depend on the details of the hardening law upon strain reversal and upon the yield function shape. The effects can be separated because the hardening model dominates at low back forces (where anticlastic curvature is minimal) and

the yield function form dominates at higher backforces approaching the force to yield the material in tension.

2. A new anisotropic hardening model reproduces well the three principal characteristics of strain hardening following a reversal of uniaxial stress: a transient region (strain range of approximately 0.01) with low yield stress and rapid work hardening, and a permanent (strain range of approximately 0.1) offset of strain or stress following reversals at higher prestrains.
3. Of the four tested yield functions (von Mises, Hill'48, Barlat YLD89, Barlat YLD96), only Barlat YLD96 faithfully reproduces springback angles, anticlastic curvatures, and oriented tensile results. The agreement of the constitutive equation combining the new hardening rule and Barlat YLD96 yield function gives remarkable agreement with all measured quantities.

Acknowledgements

The financial support of a PNGV subcontract via NIST/ATP and the Center for Advanced Materials and Manufacturing of Automotive Components (CAMMAC) is gratefully acknowledged. Experimental data for the draw-bend tests were provided by William Carden and D.K. Matlock. The uniaxial tensile test data and in-plane compression/tension test data were provided by Y. Shen and V. Balakrishnan. M.L. Wenner and F. Barlat provided many helpful discussions and encouragement. Computer time was provided by the Ohio Supercomputer Center (PAS 080). The author would like to thank Christine D. Putnam for proofreading and editing assistance.

References

- [1] Tang S. Trends on simulation of sheet metal forming processes. SAE Paper No. 2000-01-1108, SAE, Inc., 2000.
- [2] Makinouchi A, Nakamachi E, Onate E, Wagoner RH. Proceedings of the Second International Conference NUMISHET'93, Numerical Simulation of 3-D Sheet Metal Forming Processes—Verification of Simulation with Experiment, Isehara, Japan, 1993.
- [3] Shen S-F, Dawson PR, editors. Proceedings of the Fifth International Conference on Numerical Methods in Industrial Forming Processes NUMIFORM '95—Simulation of Materials Processing: Theory, Methods and Applications. Rotterdam: Balkema, 1995.
- [4] Mattiasson K, Thilderkvist P, Strange A, Samuelsson A. Simulation of springback in sheet metal forming. In: Shen S-F, Dawson PR, editors. Simulation of materials processing: theory, methods and applications. Rotterdam: Balkema, 1995. p. 115–24.
- [5] Wagoner RH, Lee JK, Kinzel G. Proceedings of the Third International Conference NUMISHET '96, Numerical Simulation of 3-D Sheet Metal Forming Processes—Verification of Simulation with Experiment, Detroit, 1996.
- [6] He N, Wagoner RH. Springback simulation in sheet metal forming. Proceedings of the Third International Conference NUMISHET '96, Numerical Simulation of 3-D Sheet Metal Forming Processes—Verification of Simulation with Experiment, Detroit, 1996.
- [7] Wagoner RH, Carden WD, Carden WP, Matlock DK. Springback after drawing and bending of metal sheets. In: Chandra T, Leclair SR, Meech JA, Verma B, Smith M, Balachandran B, editors. Proceedings of the IPMM'97—Intelligent Processing and Manufacturing of Materials, vol. 1, University of Wollongong, 1997. Brisbane, AU: Watson Ferguson & Co., 1997. p. 1–10.
- [8] Huelink J, Baaijens FPT, editors. Proceedings of the Sixth International Conference on Numerical Methods in Industrial Forming Processes NUMIFORM '98—Simulation of Materials Processing: Theory, Methods and Applications. Rotterdam: Balkema, 1998.

- [9] Focellese A, Fratini L, Gabrielli F, Micari F. The evaluation of springback in 3D stamping and coining processes. *Journal of Materials Processing Technology* 1998;80–81:108–12.
- [10] Lee SW, Yang DY. An assessment of numerical parameters influencing springback in explicit finite element analysis of sheet forming process. *Journal of Materials Processing Technology* 1998;80–81:60–7.
- [11] Li KP, Geng LM, Wagoner RH. Simulation springback with the draw/bend test. In: Meech J, editor. *Proceedings of IPMM'99, The Second International Conference on Intelligent Processing and Manufacturing of Materials*, vol. 1. New York: IEEE, 1999. p. 91–104.
- [12] Wenner ML. On work-hardening and springback in plane strain draw forming. *Journal of Applied Metalworking* 1983;2(4):277–86.
- [13] Mickalich MK, Wenner ML. Calculation of springback and its variation in channel forming operations. SAE Paper 880526, Special Publication P-206, *Advances and trends in Automotive Sheet Metal Stamping*, SAE, 1998. p. 99–110.
- [14] Zhang ZT, Lee D. Effect of process variables and material properties on the springback of 2D-draw bending parts. SAE Paper 950692, in SP-1067. Warrendale, PA: Society of Automotive Engineers, 1995. p. 11–18.
- [15] Hosford WF, Caddell RM. *Metal forming, mechanics and metallurgy*, 2nd ed. Englewood Cliffs, NJ: PTR Prentice-Hall, 1993.
- [16] Chakhari ML, Jalinier JM. Springback of complex bent parts. *Proceedings of the 13th Biennial Congress International Deep Drawing Research Group: Efficiency in Sheet Metal Forming*, Melbourne, Australia, 1984.
- [17] Fenoglietto F, Morestin F, Boivin M, Deng X. Springback analysis in orthotropic sheet metal forming with an elasto plastic formulation using a kinematic hardening model. In: Shen S-F, Dawson PR, editors. *Simulation of materials processing: theory, methods and applications*. Rotterdam: Balkema, 1995. p. 699–704.
- [18] Morestin F, Boivin M, Silva C. Elasto plastic formulation using a kinematic hardening model for springback analysis in sheet metal forming. *Journal of Materials Processing Technology* 1996;56:619–30.
- [19] Morestin F, Boivin M. On the necessity of taking into account the variation in the Young modulus with plastic strain in elastic–plastic software. *Nuclear Engineering and Design* 1996;161:107–16.
- [20] Mochida T, Taya M, Lloyd DJ. Fracture of particles in a particle/metal matrix composite under plastic straining and its effect on the Young's modulus of the composite. *Materials Transactions, JIM* 1991;32(10):931–42.
- [21] Hosford W. *The mechanics of crystals and textured polycrystals*. Oxford: Oxford Science Publications, 1993.
- [22] Barlat F. Crystallographic texture, anisotropic yield surfaces and forming limits of sheet metals. *Materials Science and Engineering* 1987;91:55–72.
- [23] Barlat F, Richmond O. Prediction of tricomponent plane stress yield surfaces and associated flow and failure behavior of strongly textured FCC polycrystalline sheets. *Materials Science and Engineering* 1987;95:15.
- [24] Taylor GI. Plastic strain in metals. *Journal of the Institute of Metals* 1938;62:307.
- [25] Bishop JWF, Hill R. A theoretical derivation of the plastic properties of a polycrystalline face-centered metal. *Philosophical Magazine* 1951;42:1298.
- [26] Hill R. Theory of yielding and plastic flow of anisotropic metals. *Proceedings of the Royal Society of London* 1948;A193:281.
- [27] Hill R. *The mathematical theory of plasticity*. Oxford: Clarendon Press, 1950.
- [28] Mellor PB, Parmar A. Plasticity of sheet metal forming. In: Koistinen DP, Wang NM, editors. *Mechanics of sheet metal forming*. New York: Plenum Press, 1978. p. 53–74.
- [29] Barlat F, Lian J. Plastic behavior and stretchability of sheet metals, Part I: a yield function for orthotropic sheets under plane stress conditions. *International Journal of Plasticity* 1989;5:51–66.
- [30] Barlat F, Maeda Y, Chung K, Yanagawa M, Brem JC, Hayashida Y, Legfe DJ, Matsui SJ, Murtha SJ, Hattori S, Becker RC, Makosey S. Yield function development for aluminum alloy sheets. *Journal of Mechanics and Physics of Solids* 1997;45(11/12):1727–63.
- [31] Hill R. Theoretical plasticity of textured aggregates. *Mathematical Proceedings of the Cambridge Society* 1979;75:179–91.
- [32] Hill R. Constitutive modeling of orthotropic plasticity in sheet metals. *Journal of Mechanics and Physics of Solids* 1990;38:405–17.
- [33] Hill R. A user-friendly theory of orthotropic plasticity in sheet metals. *International Journal of Mechanical Sciences* 1993;35:19–25.

- [34] Hershey AV. The plasticity of an isotropic aggregate of anisotropic face centered cubic crystals. *Journal of Applied Mechanics, Transactions of the ASME* 1954;21:241–9.
- [35] Hosford WF. A generalized isotropic yield criterion. *Journal of Applied Mechanics, Transactions of the ASME* 1972;39:607–9.
- [36] Logan RW, Hosford WF. Upper-bound anisotropic yield locus calculations assuming $\langle 111 \rangle$ pencil glide. *International Journal of Mechanical Sciences* 1980;22:419–30.
- [37] Hosford WF. *The plasticity of crystal and polycrystals*. Oxford: Oxford University Press, 1992.
- [38] Hosford WF. On the crystallographic basis of yield criteria. *Textures and Microstructures* 1996;26–27:479–93.
- [39] Hosford WF. On yield loci of anisotropic cubic metals. *Proceedings of the Seventh North American Metalworking Conference SME, Dearborn, MI, 1979*. p. 191–7.
- [40] Hosford WF. Comments on anisotropic yield criteria. *International Journal of Mechanical Sciences* 1985;27:423–7.
- [41] Barlat F, Lian J. Plastic behavior and stretchability of sheet metals. Part I: a yield function for orthotropic sheets under plane stress conditions. *International Journal of Plasticity* 1989;5:51.
- [42] Barlat F, Lege DJ, Brem JC. A six-component yield function for anisotropic materials. *International Journal of Plasticity* 1991;7:693–712.
- [43] Barlat F, Becker RC, Hayashida Y, Maeda Y, Yanagawa M, Chung K, Brem JCC, Lege DJ, Matsui K, Murtha SJ, Hattori S. Yielding description of solution strengthened aluminum alloys. *International Journal of Plasticity* 1997;13:385–401.
- [44] Karafillis AP, Boyce MC. A general anisotropic yield criterion using bounds and a transformation weighting tensor. *Journal of Mechanics and Physics of Solids* 1993;4:1859–86.
- [45] Yoon JW, Barlat F, Dick RE. Sheet metal forming simulation for aluminum alloy sheets. *SAE Technical Paper* 2000-01-0774, sp-1536, SAE Inc., 2000.
- [46] Banabic D, Muller W, Pohlandt K. Anisotropic yield surfaces and forming limits of sheet metals. *Proceedings of the Numisheet '99, 1999*. p. 419–24.
- [47] Banabic D, Balan T, Comsa DS, Muller W, Pohlandt K. Proposal of a new anisotropic yield criterion. *Proceedings for IDRRG, 2000*.
- [48] Banabic D, Balan T, Comsa DS, Muller W, Pohlandt K. Experimental validation of a new anisotropic yield criterion. *Proceedings for Third ESAFORM Conference on Material Forming, 2000*.
- [49] Banabic D, Kuwabara T, Balan T. Experimental validation of some anisotropic yield criteria. *Proceedings for VIIth National Conference on Technologies and Machine-Tools for cold metal forming, 2000*.
- [50] Lademo OG, Hopperstad OS, Langseth M. An evaluation of yield criteria and flow rules for aluminum alloys. *International Journal of Plasticity* 1999;15:191–208.
- [51] Choi SH, Cho JH, Barlat F, Chung K, Kwon JW, Oh KH. Prediction of yield surfaces of textured sheet metals. *Metallurgical and Materials Transactions A* 1999;30A:337–86.
- [52] Harder J. A crystallographic model for the study of local deformation process in polycrystals. *International Journal of Plasticity* 1999;15:605–24.
- [53] Miller MP, Harley EJ, Bammann DJ. Reverse yield experiments and internal variable evolution in polycrystalline metals. *International Journal of Plasticity* 1999;15:93–117.
- [54] Sowerby R, Uko DK, Tomita Y. A review of certain aspects of the Bauschinger effect in metals. *Materials Science and Engineering* 1979;41:43–58.
- [55] Abel A. Historical perspectives and some of the main features of the Bauschinger effect. *Materials Forum* 1987;10(1):11–26.
- [56] Mughrabi H. Johann Bauschinger, pioneer of modern materials testing. *Materials Forum* 1987;10(1):5–10.
- [57] Naghdi PH, Essenburg F, Koff W. An experimental study of initial and subsequent yield surfaces in plasticity. *Journal of Applied Mechanics* 1957;25:201–9.
- [58] Hu LW, Bratt JF. Effect of tensile plastic deformation on yield conditions. *Journal of Applied Mechanics* 1958;25:411.
- [59] Gill SS, Parker J. Plastic stress–strain relationships: some experiments on the effect of loading paths and loading history. *Journal of Applied Mechanics* 1959;26:77–87.
- [60] Ivey HJ. Plastic stress–strain relations and yield surfaces for aluminum alloys. *Journal of Mechanical Engineering and Sciences* 1961;3:15–31.

- [61] Parker J, Kettlewell J. Plastic stress–strain relationships; further experiments on the effect of loading history. *Journal of Applied Mechanics* 1961;28:671–82.
- [62] Miastkowski J, Szczepinski W. An experimental study of yield surfaces of prestrained brass. *International Journal of Solids and Structures* 1965;1:189–94.
- [63] Phillips A, Tang JL. The effect of loading path on the yield surface at elevated temperatures. *International Journal of Solids and Structures* 1972;8:463–74.
- [64] Helling DE, Miller AK, Stout MG. An experimental investigation of yield loci of 1100-O aluminum, 70:30 Brass, and an overaged 2024 aluminum alloy. *ASME Journal of Engineering Materials and Technology* 1986;108:313–20.
- [65] Wu HC, Yeh WC. On the experimental determination of yield surfaces and some results of annealed 302 stainless steel. *International Journal of Plasticity* 1991;7:803–26.
- [66] Eisenberg MA, Yen CF. The anisotropic deformation of yield surfaces. *ASME Journal of Engineering Materials and Technology* 1984;106:355.
- [67] Rees DW. An examination of yield surface distortion and translation. *Acta Mechanica* 1984;52:15.
- [68] Ishikawa H. Subsequent yield surface probed from its current center. *International Journal of Plasticity* 1997;13(6–7):533–49.
- [69] Wooley RL. The Bauschinger effect in some face-centered and body centered cubic metals. *Philosophical Magazine Series* 1953;7(44):597–618.
- [70] Buckley SN, Entwistle KM. The Bauschinger effect in super-pure aluminum single crystals and polycrystals. *Acta Metallurgica* 1956;4:352–61.
- [71] Orowan E. Causes and effects of internal stresses. In: Rassweiler GM, Grube WM, editors. *Internal stresses and fatigue in metals*. Amsterdam: Elsevier, 1958. p. 59–80.
- [72] Wadsworth NJ. Work hardening of copper crystals under cyclic loading. *Acta Metallurgica* 1963;11:663.
- [73] Wilson DV, Konnam YA. Work hardening in a steel containing a coarse dispersion of cementite particles. *Acta Metallurgica* 1964;12:617–28.
- [74] Wilson DV. Reversible work hardening in alloys of cubic metals. *Acta Metallurgica* 1965;13:807–14.
- [75] Svensson NL. Anisotropic and the Bauschinger effect in cold rolled aluminum. *Journal of Mechanical and Engineering Sciences* 1966;8:162–72.
- [76] Brown RC, Horne GT. The Bauschinger effect and cyclic hardening in copper. *Metallurgical Transactions* 1971;2:1161–72.
- [77] Hecker SS. Yield surface in prestrained aluminum and copper. *Metallurgical Transactions* 1971;2:2077–86.
- [78] Abel A, Muir H. The Bauschinger effect and discontinuous yielding. *Philosophical Magazine Series* 1972;8(26):489–504.
- [79] Kishi T, Tanabe T. The Bauschinger effect and its role in mechanical anisotropy. *Journal of the Mechanics and Physics of Solids* 1973;21:303–15.
- [80] Hecker SS. Influence of deformation history on the yield locus and stress–strain behavior of aluminum and copper. *Metallurgical Transactions* 1973;4:985–9.
- [81] Atkinson JD, Brown LM, Stobbs WM. The work-hardening of copper–silica IV. The Bauschinger effect and plastic relaxation. *Philosophical Magazine Series* 1974;8(30):1247–80.
- [82] Hasegawa T, Yakou T. Region of constant flow stress during compression of aluminum polycrystals prestrained by tension. *Scripta Metallurgica* 1974;8:951–4.
- [83] Lipkin J, Swearengen JC. On the subsequent yielding of an aluminum alloy following cyclic prestraining. *Metallurgical Transactions A* 1975;6A:167–77.
- [84] Lloyd DJ. The Bauschinger effect in polycrystalline aluminum containing coarse particles. *Acta Metallurgica* 1977;25:459–66.
- [85] Hasegawa T, Yakou T, Karashima S. Deformation behavior and dislocation structures upon stress reversal in polycrystalline aluminum. *Materials Science and Engineering* 1975;20:267–76.
- [86] Moan GD, Embury JD. A study of the Bauschinger effect in Al–Cu alloys. *Acta Metallurgica* 1979;22:903–14.
- [87] Anand L, Gurland J. Strain-hardening of spheroidized high carbon steels. *Acta Metallurgica* 1976;24:901–9.
- [88] Chang YW, Asaro RJ. Bauschinger effects and work-hardening in spheroidized steels. *Metal Science* 1978;12:277–84.
- [89] Bate PS, Wilson DV. Analysis of the Bauschinger effect. *Acta Metallurgica* 1986;34:1097–105.

- [90] Christodolou N, Woo OT, MacEwen SR. Effect of stress reversals on the work hardening behavior of polycrystalline copper. *Acta Metallurgica* 1986;34:1553–62.
- [91] Hasegawa T, Yakou T, Kocks UF. A unified representation of stress–strain curves in reversed direction of prestrained cell-forming metals. *Transactions of the Japan Institute of Metals* 1986;27:425–33.
- [92] Wilson DV, Bate PS. Reversibility in the work hardening of spheroidised steels. *Acta Metallurgica* 1986;34:1107–20.
- [93] Stout MG, Rollett AD. Large strain Bauschinger effects in fcc metals and alloys. *Metallurgical Transactions A* 1990;21A:3201–13.
- [94] White CS, Bronkhorst CA, Anand L. Improved isotropic-kinematic hardening model for moderate deformation plasticity. *Mechanics of Materials* 1990;10(1–2):127–47.
- [95] Giese A, Estrin Y. Mechanical behavior and microstructure of fatigued aluminum single crystals. *Scripta Metallurgica Materinlia* 1993;28:803.
- [96] Thakur A, Vecchio KS, Nemat-Nasser S. Bauschinger effect in Haynes 230 alloy: influence of strain rate and temperature. *Metallurgical Transactions A* 1996;27A:1739–48.
- [97] Miyachi K. A proposal of a planar simple shear test in sheet metals. *Scientific Papers of the Institute of Physical and Chemical Research* 1084;78(3):27–40.
- [98] Vreede P. A finite element method for simulations of 3-dimensional sheet metal forming. Enschede, The Netherlands: University of Twente, 1992.
- [99] Hoge KG, Brady RL, Cortez R. A tension–compression test fixture to determine Bauschinger effect. *Journal of Testing and Evaluation* 1973;1(4):288–90.
- [100] Tan Z, Magnusson C, Persson B. Bauschinger effect in compression–tension of sheet metals. *Materials Science and Engineering A: Structural Materials: Properties, Microstructure and Processing* 1994;A183(1–2):31–8.
- [101] Kuwabara T, Morita Y, Miyashita Y, Takahashi S. Elastic–plastic behavior of sheet metal subjected to in-plane reverse loading. In: Tanimura S, Khan AS, editors. *Proceedings of Plasticity '95, Dynamic Plasticity and Structural Behaviors, the Fifth International Symposium on Plasticity and its Current Application*. Luxembourg: Gordon and Breach, 1995. p. 841–4.
- [102] Balakrishnan V. Measurement of in-plane Bauschinger effect in metal sheets. Masters thesis, The Ohio State University, 1999.
- [103] Mroz Z. On the description of anisotropic work hardening. *Journal of Mechanics and Physics of Solids* 1967;15:163–75.
- [104] Mroz Z. An attempt to describe the behavior of metals under cyclic loads using a more general workhardening model. *Acta Mechanica* 1969;7:1990–2122.
- [105] Dafalias YF, Popov EP. Plastic internal variables formalism of cyclic plasticity. *Journal of Applied Mechanics* 1976;98:645–51.
- [106] Krieg RD. A practical two surface plasticity theory. *Journal of Applied Mechanics, Transactions of the ASME* 1975;47:641–6.
- [107] Armstrong PJ, Frederick CO. A mathematical representation of the multiaxial Bauschinger effect. G.E.G.B. Report RD/B/N 731, 1966.
- [108] Chaboche JL, Dang Van K, Cordier G. Modelization of the strain memory effect on the cyclic hardening of 316 stainless steel. *Trans SMiRT-S, Div. L, Berlin, L11/3*, 1979.
- [109] Ristinmaa M. Cyclic plasticity model using one yield surface only. *International Journal of Plasticity* 1995;11(2):163–81.
- [110] Jiang Y, Kurath P. Characteristics of the Armstrong–Frederick type plasticity models. *International Journal of Plasticity* 1996;12(3):387–415.
- [111] Chaboche JL. Time-independent constitutive theories for cyclic plasticity. *International Journal of Plasticity* 1986;2(2):149–88.
- [112] Petersson H, Popov EP. Constitutive equations for generalized loadings. *Journal of Engineering Mechanics Division ASCE* 1977;104:611.
- [113] Dafalias YF. Modeling cyclic plasticity: Simplicity versus sophistication. In: Desai CS, Gallagher RH, editors. *Mechanics of engineering materials*. New York: Wiley, 1984. p. 153–78.
- [114] Khan A, Huang SH. *Continuum theory of plasticity*. New York: Wiley, 1995.

- [115] Chaboche JL. Cyclic plasticity modeling and ratchetting effects. In: Desai CS, et al., editors. *Proceedings of the Second International Conference on Constitutive Laws for Engineering Mater: Theory and Applications*, Tucson, Arizona. Amsterdam: Elsevier, 1987. p. 47–58.
- [116] Chaboche JL. On some modifications of kinematic hardening to improve the description of ratchetting effects. *International Journal of Plasticity* 1991;7:661.
- [117] Chaboche JL, Rousselier G. On the plastic and viscoplastic constitutive equations, Parts I and II. *Journal of Pressure Vessel Technology* 1983;105–53.
- [118] Chaboche JL, Nouailhas D. Constitutive modeling of ratchetting effects—Part I: experimental facts. *ASME Journal of Engineering and Materials Technology* 1989;111:384.
- [119] Ohno N, Wang JD. Nonlinear kinematic hardening rule with critical state for activation of dynamic recovery. In: Boehler J-P, Khan AS, editors. *Proceedings of the Plasticity '91; Third International Symposium on Plasticity and its Current Applications*, Grenoble, France. Essex, UK: Elsevier Science, 1991. p. 455–8.
- [120] Ohno N, Wang JD. Kinematic hardening rules with critical state of dynamic recovery: Part I-formulation and basic features for ratchetting behavior. *International Journal of Plasticity* 1993;9:375.
- [121] Ohno N, Wang JD. Kinematic hardening rules with critical state of dynamic recovery: Part II: application to experiments of ratchetting behavior. *International Journal of Plasticity* 1993;9:391.
- [122] Jiang Y, Sehitoglu H. Modeling of cyclic ratchetting plasticity, Part I: development of constitutive relations. *Journal of Applied Mechanics* 1995;63:720–5.
- [123] Jiang Y, Sehitoglu H. Modeling of cyclic ratchetting plasticity, Part II: comparison of model simulations with experiments. *Journal of Applied Mechanics* 1995;63:726–33.
- [124] Ohno N, Kachi Y. A constitutive model of cyclic plasticity for nonlinear hardening materials. *ASME Journal of Applied Mechanics* 1986;53:395–403.
- [125] Ohno N, Satra M. Detailed and simplified elastoplastic analysis of a cyclically loaded notched bar. *ASME Journal of Engineering and Materials Technology* 1987;109:194–202.
- [126] Bower AF. Cyclic hardening properties of hard-drawn copper and rail steel. *Journal of Mechanics and Physics of Solids* 1989;37:455.
- [127] Geng LM, Wagoner RH. Springback analysis with a modified hardening model. SAE Technical Paper 2000-01-0768, *Sheet Metal Forming: Sing Tang 65th Anniversary Volume*, SP-1536, SAE, 2000.
- [128] Hodge PG. A new method of analyzing stresses and strains in work hardening plastic solids. *Journal of Applied Mechanics* 1957;24:482–3.
- [129] Crisfield MA. *Non-linear finite element analysis of solids and structures. Advanced topics*, vol. 2. New York: Wiley, 1991.
- [130] Vallance DW, Matlock DK. Application of the bending-under-tension friction test to coated sheet steels. *Journal of Material Engineering and Performance* 1992;1(5):685–93.
- [131] Wagoner RH, Carden WD, Carden WP, Matlock DK. Springback after drawing and bending of metal sheets. In: Chandra T, Leclair SR, Meech JA, Verma B, Smith M, Balachandran B, editors. *Proceedings, IPMM '97 - Intelligent Processing and Manufacturing of Materials*, University of Wollongong, 1997. p. 1–10.
- [132] Carden WD. Springback after drawing and bending of metal sheets. MS thesis, The Ohio State University, 1997.
- [133] Carden WD, Geng LM, Matlock DK, Wagoner RH. Measurement of springback. *International Journal of Mechanical Sciences* 2002;44:79–101.
- [134] Shen Y. The reverse-bend test: indirect measurement of the Bauschinger effect in metal sheets. MS thesis, The Ohio State University, 1999.
- [135] Barlat F. Report for NIST-ATP/SPP Project, 1997.
- [136] Prager W. A new method of analyzing stresses and strains in work hardening plastic solids. *Journal of Applied Mechanics* 1956;23:493–6.
- [137] User's manual, ABAQUS/Standard version 5.8. Pawtucket, RI: Hibbit, Karlsson & Sorensen Inc., 1998.
- [138] Yu TX, Zhang LC. *Plastic bending, theory and applications*. Singapore: World Scientific, 1996.
- [139] Horrocks D, Johnson W. On anticlastic curvature with special reference to plastic bending: a literature survey and some experimental investigations. *International Journal of Mechanical Sciences* 1967;8:835–61.
- [140] Li KP, Carden WP, Wagoner RH. Simulation of springback. *International Journal of Mechanical Sciences* 2002;44:103–22.

- [141] Li K, Wagoner RH. Simulation of springback. In: Huetink J, Baaijens FPT, editors. *Simulation of materials processing*. Rotterdam: A.A. Balkema, 1998. p. 21–32.
- [142] Li K, Geng L, Wagoner RH. In: Geiger M, editor. *Simulation of springback: choice of element, advanced technology of plasticity 1999*, vol. III. Berlin: Springer, 1999. p. 2091–8.